Fabrication of the planar angular rotator using the CMOS process

2002 J. Micromech. Microeng. 12 247

(http://iopscience.iop.org/0960-1317/12/3/308)

INSTITUTE OF PHYSICS PUBLISHING JOURNAL OF MICROMECHANICS AND MICROENGINEERING

J. Micromech. Microeng. **12** (2002) 247–251 PII: S0960-1317(02)28571-X

Fabrication of the planar angular rotator using the CMOS process

Ching-Liang Dai[1], Chien-Liu Chang[2], Hung-Lin Chen[2] and Pei-Zen Chang[2]

[1] Department of Mechanical Engineering, Oriental Institute of Technology, Taipei 220, Taiwan, Republic of China

[2] Institute of Applied Mechanics, National Taiwan University, Taipei 107, Taiwan, Republic of China

E-mail: fd032@ica.oit.edu.tw

Received 5 September 2001, in final form 14 January 2002
Published 28 March 2002
Online at stacks.iop.org/JMM/12/247

Abstract

In this investigation we propose a novel planar angular rotator fabricated by the conventional complementary metal–oxide semiconductor (CMOS) process. Following the 0.6 μm single poly triple metal (SPTM) CMOS process, the device is completed by a simple maskless, post-process etching step. The rotor of the planar angular rotator rotates around its geometric center with electrostatic actuation. The proposed design adopts an intelligent mechanism including the slider–crank system to permit simultaneous motion. The CMOS planar angular rotator could be driven with driving voltages of around 40 V. The design proposed here has a shorter response time and longer life, without problems of friction and wear, compared to the more common planar angular micromotor.

1. Introduction

Microelectromechanical systems (MEMS) have received increasing interest in recent years. Various fabrication technologies, including LIGA, and surface and bulk micromachining, have been developed to fulfill specific industrial requirements. However, the specialized processes may not automatically allow for on-chip integration of MEMS devices and integrated circuits. Therefore, developing a MEMS structure compatible with a commercially available complementary metal–oxide semiconductor (CMOS) [1, 2] process has also received extensive interest. Many microsensors [3–5] and microactuators [6–8] have been fabricated using the CMOS process.

The most common planar rotor actuated in-plane is the micromotor, proposed by many researchers [9]. Related applications of the micromotor include optical switches [10], microgear [11] and microengines [12]. However, the friction [13] and wear of the micromotor restrict the response speed and lifetime. Researchers have also reported on another type of rotator operated at limited angles. The rotary units are supported by flexure suspensions, making friction and wear problems avoidable. The mechanism is useful for the heads of hard disk devices to employ the characterization of quick response [14]. The planar angular rotator suggested herein belongs to this latter type.

In light of the above developments, in this paper we present a planar angular rotator fabricated by the conventional CMOS process. The rotor could be actuated by electrostatic force. The benefits of actuation are without wear and friction

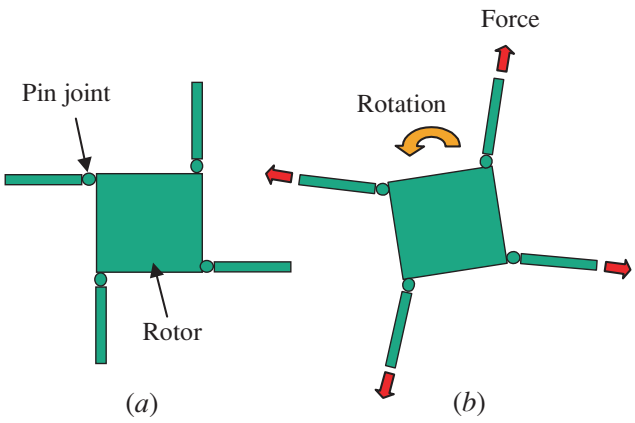

Figure 1. The rotor of the planar angular rotator: (*a*) without actuation, and (*b*) with actuation.

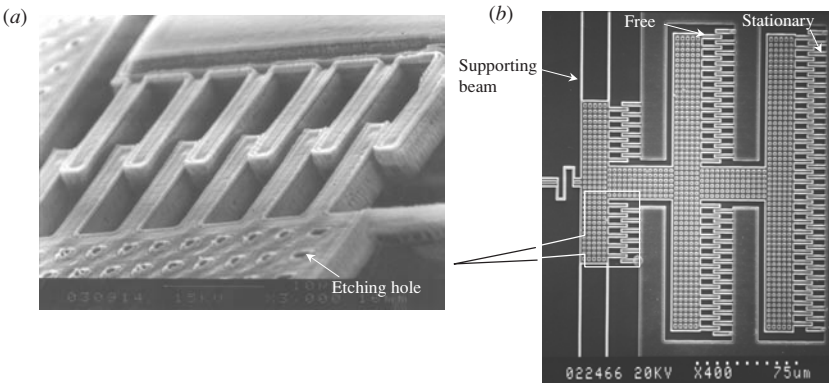

Figure 2. Scanning electron micrographs of the comb structure: (*a*) partial magnification and (*b*) three rows of comb fingers.

problems. In this paper we also describe the configuration of the microactuator and the novelty of the kinetic behavior.

2. Operating principle

2.1. Actuating mechanism

The actuating principle of the planar angular rotator can be derived intuitively from figure 1. Figure 1(*a*) indicates that a suspended rotor is supported by four beams via the pin-joint-like [15] connectors. According to figure 1(*b*), with electrostatic force, the beams are pulled outwards, the connectors acting as rollers, and then the rotor rotates around its center.

The electrostatic driving force generated from the comb structure is related to the applied voltage, the dielectric constant, the gap between two fingers and the height and number of fingers. Since the dielectric constant regarding the medium (air) herein is essentially fixed, smaller gaps, greater height and more fingers are necessary for decreasing the voltage demand with large force. Corresponding to the design rule of the CMOS process, the gap could be as small as 0.8 μm. Meanwhile, this study develops a laminated structure [16] to meet the height requirement. By stacking the three metal and two oxide layers, the total height is raised to 5 μm. Additionally, this investigation designs three rows of comb structures to increase the number of fingers to 66 pairs as shown in figure 2.

2.2. Slider–crank mechanism

For the practical devices, figure 3 illustrates the scanning electron micrograph of the CMOS planar angular rotator. With the electrical potential, the comb structure will be pulled in the direction parallel to the capacitance plate. Additionally, the S-shaped flexures are joined to the ends of the transmission bar as depicted in figures 4(*a*) and (*b*). Because the flexures are thinner and softer than the transmission bar, the deformation occurs at the S-shaped flexures and tilts the transmission bar. Subsequently, the rectilinear motion of the comb would be translated into the rotatory motion of the suspended unit via the transmission bar. The driving mechanism of the rotator, in sum, is a slider–crank system.

As figure 4(*c*) reveals, the relation between slider and crank includes sliding displacement, x, and rotatory angle, Δ.

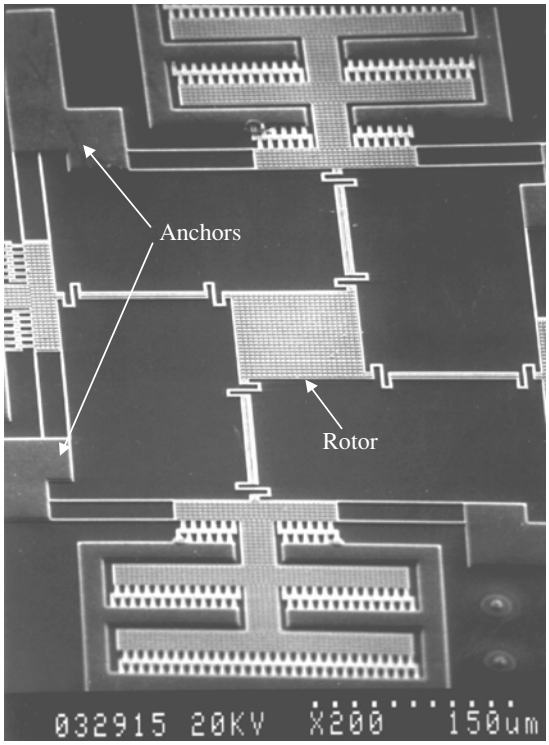

Figure 3. Scanning electron micrograph of the CMOS planar angular rotator.

The equation of motion [17] could be expressed as

$$x = R[\cos\theta - \cos(\theta + \Delta)] + \frac{R^2}{2L}[\sin(\theta + \Delta) - \sin\theta] \quad (1)$$

where θ is the initial angle from the horizontal, L is the length of the connecting rob and R is the crank length. In practical design, θ equals 45°, L is the length of the transmission bar and equals 100 μm and R is the half diagonal length of the rotor.

According to equation (1), the motion could be calculated and plotted with the various half diagonal lengths of the rotor as shown in figure 4(*d*). The plot obviously reveals that more displacement is required for the larger unit at the same rotatory angle. To reduce the demand of actuating distance, in this investigation we suggest an array of small units to serve as a big unit.

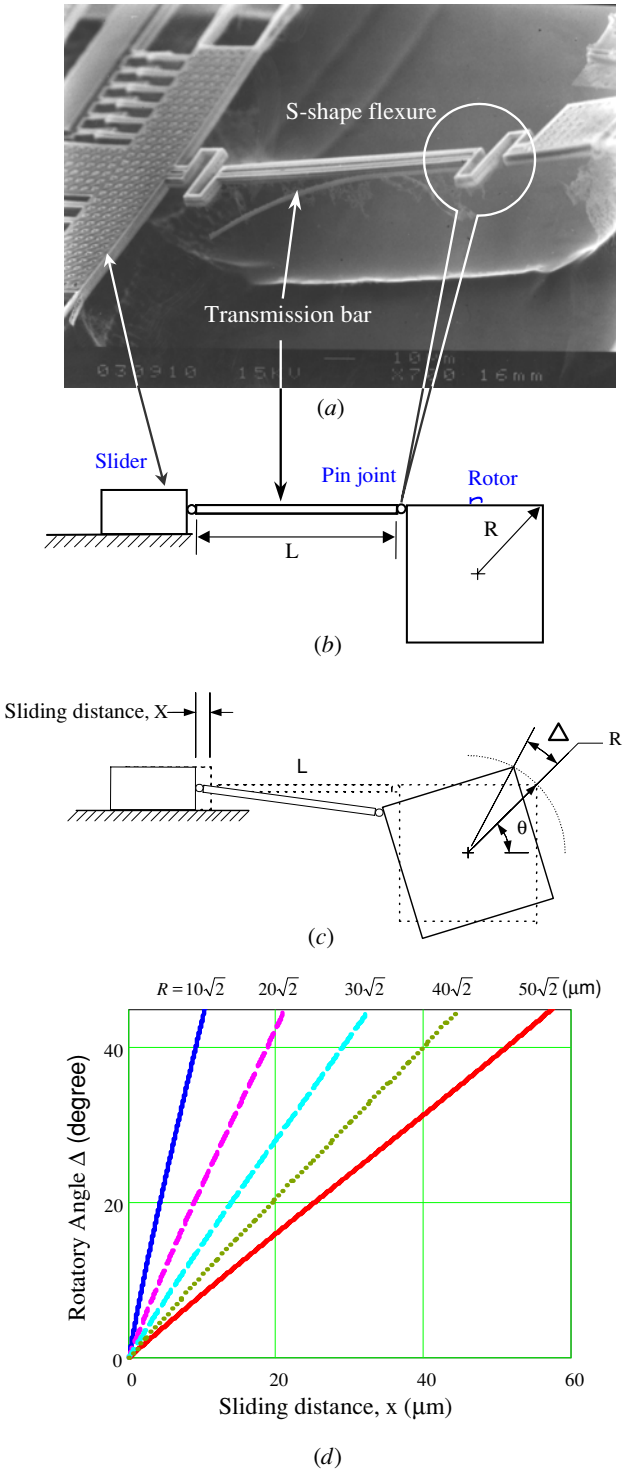

Figure 4. Slider–crank mechanism: (*a*) scanning electron micrograph, (*b*) equivalent model, (*c*) schematic diagram and (*d*) plot of sliding distance and rotatory angle for different half diagonal lengths (R).

3. Fabrication

The design of the planar angular rotator is in accord with the 0.6 μm single poly and triple metal (SPTM) foundry service of Taiwan Semiconductor Manufacture Company (TSMC).

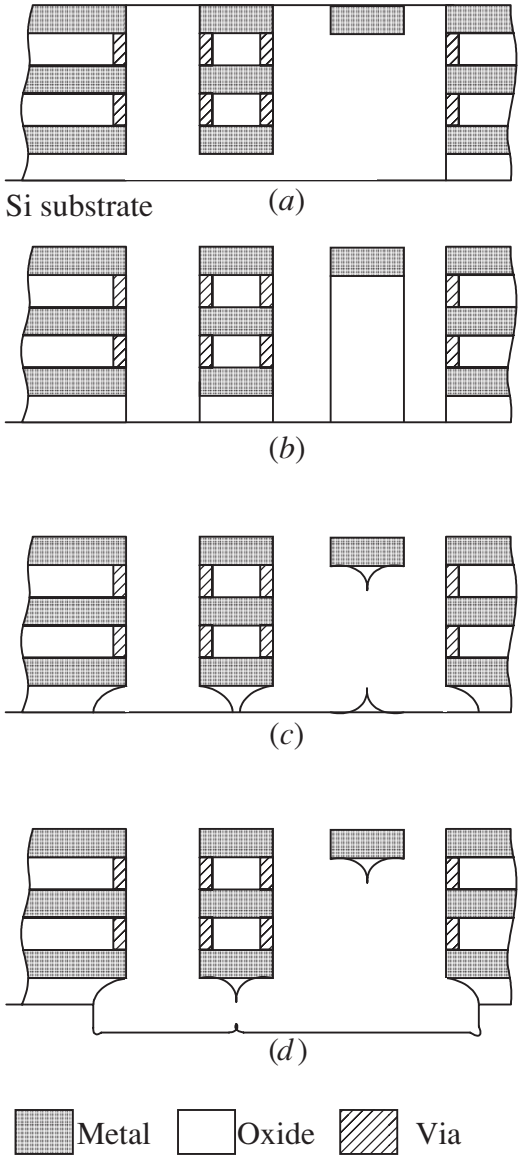

Figure 5. Schematic cross-section view of the post-CMOS process sequence: (*a*) following the CMOS foundry service, (*b*) anisotropic silicon dioxide etching, (*c*) isotropic silicon dioxide etching and (*d*) isotropic silicon etching.

Following the foundry service, a simple post-process with maskless etching releases the structure.

The post-process includes three steps to release the structure. Figure 5(*a*) presents the schematic cross-section view after the foundry service. All the passivation nitride is already removed and the metal layer is exposed. Although this violates the design rules that require the top metal layer to exist when the passivation nitride is absent, the process still works from the point of microfabrication. Figure 5(*b*) depicts the anisotropic oxide etching through the silicon substrate by CF_4/O_2 reactive ion etching (RIE). Although most of the structure is constructed with the laminated layers, the soft parts are only defined by a single metal layer. Accordingly, isotropic silicon dioxide etching is needed to release the soft parts, as shown in figure 5(*c*), and this step could be completed by NF_3 RIE or concentrated HF (49%) wet etching [18]. Figure 5(*d*) shows the silicon substrate etching for releasing the

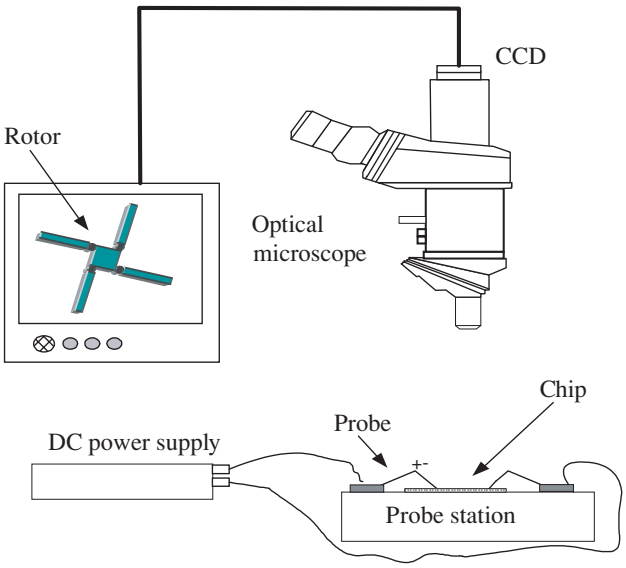

Figure 6. Schematic diagram of the experimental setup for the planar angular rotator.

whole structure. To employ the large undercut of the SF_6 RIE, 3 μm width of the beam could be released in 20 min by plasma etching. Furthermore, although a higher gas pressure can make the plasma etching more isotropic, when the pressure is too high the etching depth becomes inconsistent.

4. Results and discussion

The experimental setup for the planar angular rotator is illustrated in figure 6. Both pads on the chip are connected respectively to the positive and negative electrodes of the power supply by probe stations. The power supply applies voltage to the comb structures generating the electrostatic driving force that rotates the rotor of planar angular rotator. The rotor could start around 40 V and rotate to 5° around 46 V. Increasing driving voltages could result in breakdown around 120 V but the rotor had no further rotation. The experiment shows that the controllable range is between 40 and 46 driving volts corresponding to 0 and 5° rotation angle. Most of the force was confined within the S-shaped flexure, and the rotor could not rotate to more than 5°. For improving the performance, a longer transmission bar and softer S-shaped flexures would be necessary to satisfy the assumptions of pin-joint-like mechanism and, in doing so, would make the motion smoother and larger.

According to the CMOS foundry service adopted herein, the via implies digging of a tunnel in the oxide layer between the two metal layers. Using the via to connect each metal layer not only expands the electrode, but also protects the structure from plasma etching (figure 5). The suspended microstructures of the planar angular rotator are made of metal layers. In order to decrease the etching time when releasing the suspended microstructures, many etching holes are designed in the suspended microstructures as shown in figure 7(*a*). The surface of the suspended microstructures is rugged owing to etching holes. However, the caves would be filled with polymer after F-based plasma etching (figure 7(*b*)). As a restatement, polymerization occurs in the

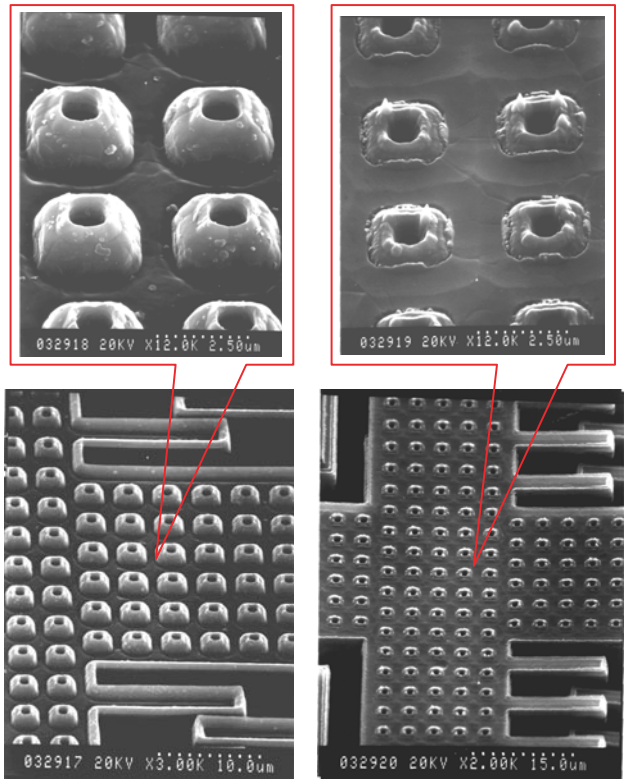

(*a*) (*b*)

Figure 7. Etching holes in the microstructures: (*a*) before etching and (*b*) after etching with polymerization.

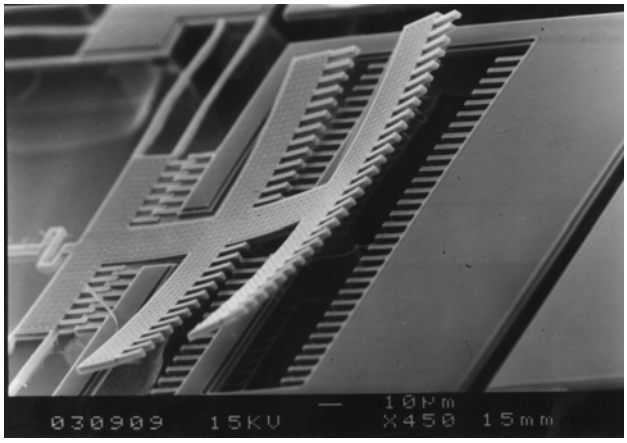

Figure 8. The free end of the structure bending out-of-plane.

metal layer, accounting for why it is a good etching mask for plasma etching [19].

Over plasma etching would cause the free structure bending out-of-plane (figure 8) due to ion bombardment-induced stress concentration on the surface. The bending potentially results in the failure of actuation or demand of more driving volts. Therefore, a precision etching time should be found to fully release the structure without bending.

Optical switches are important components for the optical fiber communication networks. Lee *et al* [20] proposed

free-space fiber-optic switches based on vertical torsion mirrors. The planar angular rotator is able to use the optical switch. TSMC recently had a single polysilion six metal (1P6M) CMOS process. The 1P6M process, which has six metal layers, can be used to fabricate three-dimensional microstructures. In future, we will fabricate vertical micro mirrors set on the rotor of the planar angular rotator using the 1P6M CMOS process. The action of the rotor can switch the direction of vertical micro mirrors as the optical switch does.

5. Conclusion

In this work we have designed and fabricated the planar angular rotator using the CMOS process. Experimentally, in this study we perform maskless etching with plasma or solvent and obtain excellent results including high selectivity and full release of the structure. Finally, the CMOS planar angular rotator could be driven by applying voltages of around 40 V. The whole procedure is simple and compatible with the integrated circuits. This investigation not only reduces the developing time, but also minimizes the scale by following the advancing CMOS process.

Acknowledgments

This work was accomplished with much needed support and the authors wish to thank Chien-Liu Chang, Jenn-yi Chen, Chi-yuan Lee, Hung-hsuan Lin, Fu-yuan Xiao, Tsung-wei Huang, Shih-Chen Chang and Chun-yuan Chi of the Institute of Applied Mechanics, National Taiwan University, for their financial support and valuable assistance in the experiment. The support of the National Chip Implementation Center is also appreciated.

References

[1] Parameswaran M, Robinson A M, Blackburn D L, Gaitan M and Geist J 1991 Micromachined thermal radiation emitter from a commercial CMOS process *IEEE Electron Device Lett.* **12** 57–9

[2] Milanovic V, Ozgur M, DeGroot D C, Jargon J A, Gaitan M and Zaghloul M E 1998 Characterization of broad-band transmission for coplanar waveguides on CMOS silicon substrates *IEEE Trans. Microw. Theory Tech.* **46** 632–40

[3] Berney H, Hill M, Cotter D, Hynes E, O'Neill M and Lane W A 2001 Determination of the effect of processing steps on the CMOS compatibility of a surface micromachined pressure sensor *J. Micromech. Microeng.* **11** 402–8

[4] Socher E, Bochobza-Degani O and Nemirovsky Y 2001 A novel spiral CMOS compatible micromachined thermoelectric IR microsensor *J. Micromech. Microeng.* **11** 574–6

[5] Robadey J, Paul O and Baltes H 1995 Two-dimensional integrated gas flow sensors by CMOS IC technology *J. Micromech. Microeng.* **5** 243–50

[6] Dai C L, Chen H L and Chang P Z 2001 Fabrication of a micromachined optical modulator using the CMOS process *J. Micromech. Microeng.* **11** 612–5

[7] Dai C L, Yen K and Chang P Z 2001 Applied electrostatic parallelogram actuators for microwave switches by standard CMOS process *J. Micromech. Microeng.* **11** 697–702

[8] Yang L J, Huang T W and Chang P Z 2001 CMOS microelectromechanical bandpass filters *Sensors Actuators* A **90** 148–52

[9] Mehregany M, Senturia S D, Lang J H and Nagarkar P 1992 Micromotor fabrication *IEEE Trans. Electron Devices* **39** 2060–9

[10] Yasseen A A, Mitchell J, Streit T, Smith D A and Mehregany M 1998 A rotary electrostatic micromotor 1×8 optical switch *MEMS'98: Proc. IEEE Micro Electro Mechanical Systems (Heidelberg, Germany, Jan. 1998)* pp 116–20

[11] Legtenberg R, Berenschot E, Elwenspoek M and Fluitman J H 1996 Electrostatic microactuators with integrated gear linkages for mechanical power transmission *MEMS'96: Proc. IEEE Micro Electro Mechanical Systems (California, USA, Feb. 1996)* pp 204–9

[12] Sniegowski J J and Garcia E J 1996 Surface-micromachined gear train driven by an on-chip electrostatic microengine *IEEE Electron Device Lett.* **17** 366–8

[13] Beerschwinger U, Reuben R L and Yang S J 1997 Frictional study of micromotor bearings *Sensors Actuators* A **63** 229–41

[14] Horsley A, Cohn M B, Singh A, Horowitz R and Pisano A P 1998 Design and fabrication of an angular microactuator for magnetic disk drives *IEEE J. Microelectromech. Syst.* **7** 141–8

[15] Fan L S, Tai Y C and Muller R S 1993 Integrated movable micromechanical structures for sensors and actuators *IEEE J. Microelectromech. Syst.* **2** 44–55

[16] Fedder K, Santhanam S, Reed M L, Eagle S C, Gullou D F, Lu M S C and Carley L R 1996 Laminated high-aspect-ratio microstructures in a conventional CMOS process *MEMS'96: Proc. IEEE Micro Electro Mechanical Systems (California, USA, Feb. 1996)* pp 13–8

[17] Martin G H 1982 *Kinematics and Dynamics of Machines* (New York: McGraw-Hill) ch 14

[18] Gennissen P T J and French P J 1997 Sacrificial oxide etching compatible with aluminum metallization *Transducers'97: Int. Conf. Solid-State Sensors and Actuators (Chicago, USA, June, 1997)* pp 225–8

[19] Jansen H, Gardeniers H, Boer M D, Elwenspoek M and Fluitman J 1996 A survey on the reactive ion etching of silicon in microtechnology *J. Micromech. Microeng.* **6** 14–28

[20] Lee S S, Huang L S, Kim C J and Wu M C 1999 Free-space fiber-optic switches based on MEMS vertical torsion mirrors *J. Lightwave Technol.* **17** 7–13